Rigorous Prediction of the Ground Wave Above Flat and Rough Highly-Conducting One-Dimensional Sea Surfaces in HF-VHF Band

Christophe Bourlier, *Member, IEEE*, Gildas Kubické, and Yohann Brelet

Abstract—For horizontally and vertically polarized line sources in HF-VHF band, a detailed analysis of the propagation over one-dimensional highly-conducting smooth and rough sea surfaces is addressed from an efficient rigorous numerical method: the method of moments combined with the BMIA-CAG approach and with the impedance boundary condition (Leontovitch approximation). This method can treat a huge problem, typically, ranging from 200 000 to 300 000 for the number of unknowns on the surface, which allows us to show, for the TM polarization, the ground wave propagation over a long distance. The contribution of the surface wave is then exhibited for a smooth sea surface and compared with the Collin asymptotic formulation deduced from the Sommerfeld integral. The surface roughness effect on the propagation is also investigated.

Index Terms—Electromagnetic scattering, ground wave, rigorous numerical methods, Sommerfeld integral.

I. INTRODUCTION

THE Sommerfeld problem of radiation of a line source above an infinite lossy half-space is a classic problem in electromagnetics that has received significant attention. However, because of its relevance in a wide range of applications, it is still being examined. Collin [1], Wait [2], Sarabandi *et al.* [3], [4] (references therein), Koh *et al.* [5] (references therein), and many other authors presented a review of this problem for the vertical and horizontal polarizations. For a rough surface, from earlier works and from an asymptotic perturbative theory (see for instance Barrick [6], [7]), Ishimaru *et al.* [8], [9] introduced the roughness effect. In addition, in the HF band (3–30 MHz), Toporkov *et al.* [10] showed that the conventional small-perturbation method must be multiplied by an attenuation function, corresponding to the contribution to the surface wave, in which the pole is modified by the surface roughness.

In the HF-VHF band (typically, Radar frequencies ranging from 1 MHz to 100 MHz), the sea surface is highly conducting, implying that the surface normalized impedance modulus $|\Delta|$ is close to zero (high surface permittivity modulus). For the ver-

tical polarization and for grazing angles, this particularity involves the existence of a surface wave, which can propagate over a long distance near the surface: the ground wave. Mathematically, this wave is due to the pole, in the Fourier domain, of the Green function, which contributes if $\cos\theta = -\Delta$, where θ is the incidence angle defined from the nadir. Since $|\Delta|$ is close to zero, $\chi = \pi/2 - \theta$ must be close to zero, corresponding to grazing angles. For horizontal polarization, such a phenomenon does not exist because the Green function pole is not excited (in this case $\cos\theta = -1/\Delta$).

For highly-conducting surfaces, the calculation of the Sommerfeld integral is a very difficult task because the integrand strongly oscillates and decreases slowly. Nevertheless, for large observation distance, a closed-form asymptotic expression of this integral can be obtained. Article [1] presents a contemporary solution of this problem and works done on this problem in the last century. One of the purpose of this paper is to compare this asymptotic solution with a rigorous solution. In addition, the surface roughness effect on the surface wave propagation is also investigated. Indeed, a very efficient numerical rigorous method, based on the Method of Moment (MoM) is used to compute the scattered field by smooth and rough surfaces and by applying the impedance boundary condition (Leontovitch approximation).

To exhibit the ground wave, the surface must be very large, a few hundreds of kilometers, which implies to solve a problem with a number of unknowns on the surface ranging from 200 000 to 300 000 for the HF-VHF band. This is impossible from a classical MoM with a LU inversion. The surface is then assumed to be 1-D.

The paper is organized as follows. For a smooth surface, Sections II and III present the problem and asymptotic solutions of the Sommerfeld integral. Section IV is devoted to the choice and the validation of the efficient rigorous method and Sections V and VI present numerical results for smooth and rough surfaces in the HF-VHF band. The last section gives concluding remarks.

II. FORMULATION OF THE PROBLEM FOR A SMOOTH SURFACE

For a one-dimensional smooth surface of infinite length, in terms of scalar Green's functions, the total field above the surface is given by [8] (the time convention $e^{-i\omega t}$ is assumed)

$$g_t(\mathbf{r}, \mathbf{r}_0) = g_i(\mathbf{r}, \mathbf{r}_0) + g_s(\mathbf{r}, \mathbf{r}_0) \tag{1}$$

where $g_i(\mathbf{r}, \mathbf{r}_0) = (i/4)H_0^{(1)}(k_0 \|\mathbf{r} - \mathbf{r}_0\|)$ is the incident field radiated by the line source located at the point $\mathbf{r}_0 = (x_0, z_0)$ and
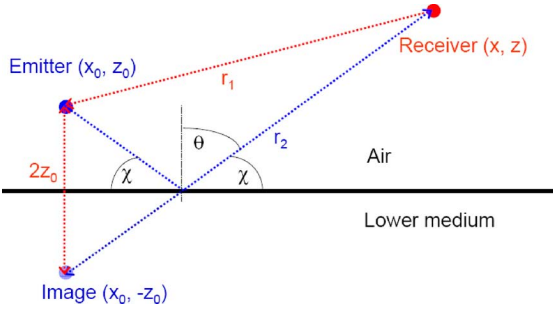
Fig. 1. Description of the problem geometry. The emitter is located at the height z_0 and the abscissa x_0. The receiver is located at the height z and the abscissa x. The image is located at the height $-z_0$ and the abscissa x_0.

$g_s(\mathbf{r}, \mathbf{r}_0)$ is the scattered field observed at the point $\mathbf{r} = (x, z)$ (see Fig. 1). The upper medium is assumed to be the vacuum ($n = 1$). The incident wave number is denoted as $k_0 = 2\pi/\lambda_0$.

From the Weyl representation, the scalar Green functions are expressed in the Fourier domain as

$$\begin{cases} g_i(\mathbf{r}, \mathbf{r}_0) = \frac{1}{2\pi} \int_{-\infty}^{+\infty} \frac{i}{2k_z} e^{ik_z|z-z_0|+ik_x(x-x_0)} dk_x \\ g_s(\mathbf{r}, \mathbf{r}_0) = \frac{1}{2\pi} \int_{-\infty}^{+\infty} \frac{i\hat{\mathcal{R}}(k_x)}{2k_z} e^{ik_z(z+z_0)+ik_x(x-x_0)} dk_x \end{cases} \quad (2)$$

where

$$k_z = \begin{cases} \sqrt{k_0^2 - k_x^2} & \text{if } k_0 \geq k_x \text{ (propagative waves)} \\ i\sqrt{k_x^2 - k_0^2} & \text{if } k_0 < k_x \text{ (evanescent waves)} \end{cases} \quad (3)$$

and the Fresnel coefficients are defined in H (TE case) and V (TM case) polarizations as

$$\begin{cases} \hat{\mathcal{R}}(k_x) = \frac{\hat{Q}(k_x)-1}{\hat{Q}(k_x)+1} & \text{with } \hat{Q}(k_x) = \frac{k_z \hat{\Delta}(k_x)}{k_0} \quad \text{(TE)} \\ \hat{\mathcal{R}}(k_x) = \frac{1-\hat{Q}(k_x)}{1+\hat{Q}(k_x)} & \text{with } \hat{Q}(k_x) = \frac{k_0 \hat{\Delta}(k_x)}{k_z} \quad \text{(TM)} \end{cases} . \quad (4)$$

The symbol $\hat{\ }$ means that the variables are expressed in the Fourier domain. Moreover, the normalized surface impedance is expressed as

$$\hat{\Delta}(k_x) = \frac{1}{n}\sqrt{1 - \frac{k_x^2}{n^2 k_0^2}} \approx \frac{1}{n}\sqrt{1 - \frac{1}{n^2}} = \Delta. \quad (5)$$

For low grazing angles, $k_x \to k_0$ and then the ratio $k_x/k_0 \to 1$. In addition, for large $|n| \gg 1$ (highly-conducting surface), the normalized surface impedance $\Delta \approx 1/n$ (it becomes independent of k_x), where n is the surface refractive index.

The substitution of (4) and (2) into (1) leads to

$$g_t(\mathbf{r}, \mathbf{r}_0) = g(r_1) \pm [g(r_2) - 2P] \quad (6)$$

where

$$P = \frac{1}{2\pi} \int_{-\infty}^{+\infty} \frac{i}{2k_z} \frac{\hat{Q}(k_x)}{1 + \hat{Q}(k_x)} e^{ik_z(z+z_0)+ik_x(x-x_0)} dk_x \quad (7)$$

and $g(r) = (i/4)H_0^{(1)}(k_0 r)$. $g(r_1)$ represents the incident field, whereas $g(r_2)$ is the incident field of the transmitter image located at the point $(x_0, -z_0)$ (see Fig. 1). In (6), the sign *plus*

refers to the TM polarization (or polarization V), whereas the sign *minus* refers to the TE polarization (or polarization H).

For a perfectly-conducting surface, $\Delta = 0$ and $P = 0$. Thus, in (6), the term $g(r_1) \pm g(r_2)$ stands for the total field by a perfectly-conducting surface.

In the following, the surface complex relative permittivity ϵ_r is assumed to be

$$\epsilon_r = \epsilon_r' + \frac{i\sigma}{2\pi f \epsilon_0} = \epsilon_r' + \frac{18 i\sigma}{f(\text{GHz})} \quad (8)$$

where σ is the conductivity in S/m, and $n = \sqrt{\epsilon_r}$. In addition, $\sigma = 4$ S/m and the real part of the relative permittivity is $\epsilon_r' = 80$, which implies that the sea complex relative permittivity is $\epsilon_r = 80 + 72i/f$, with f in GHz.

III. EVALUATION OF THE SOMMERFELD INTEGRAL

From (7) and (4), a pole occurs at $\hat{Q}(k_x) = -1$, giving $k_{zp} = -k_0/\Delta$ for the TE polarization and $k_{zp} = -k_0\Delta$ for the TM polarization. For a highly-conducting surface, since $|\Delta| \to 0$, the pole does not contribute for the TE polarization (in this case $|k_{zp}/k_0| \gg 1$), whereas for the TM polarization, the pole can contribute because $|k_{zp}/k_0| \ll 1$, corresponding to grazing angles. Thus, the evaluation of integral (7) is not straightforward for the TM polarization because a pole occurs in the integrand. For a 2-D surface, a detailed analysis of several asymptotic derivations published in the previous century is addressed in recent papers of Collin [1] and Koh *et al.* [5]. See also the article of Wait [2]. In addition, for a highly-conducting surface ($|n| \gg 1$), like the sea surface in HF-VHF band, the modulus of the normalized surface impedance ($|\Delta| \approx 1/|n|$) is close to zero, which makes the computation of the integral very difficult.

For the TE polarization, we show in Appendix A that

$$P = -\frac{i}{4} \sum_{n=1}^{\infty} \left(\frac{i\Delta}{k_0}\right)^n \frac{\partial^n}{\partial z_2^n} H_0^{(1)}\left(k_0\sqrt{x_2^2 + z_2^2}\right) \quad (9)$$

where $x_2 = x - x_0$ and $z_2 = z + z_0$. For a highly-conducting surface ($|\Delta| \to 0$) and unlike the TM polarization, the series converge very rapidly. We then show that

$$P \approx -\frac{\Delta \cos\theta}{4} H_1^{(1)}\left(k_0\sqrt{x_2^2 + z_2^2}\right) \Rightarrow P^\infty \approx g^\infty(r_2)\Delta\cos\theta \quad (10)$$

for $k_0 r_2 \gg 1$ and $|\Delta| \to 0$. In addition, $g^\infty(r_2) = i\sqrt{2/(\pi k_0 r_2)}e^{i(k_0 r_2 - \pi/4)}/4$ is the scalar Green function in the far field zone. For $\chi = \pi/2 - \theta \to 0$, (10) behaves as $\Delta\chi$. This explains clearly that for the TE polarization, a surface wave can not propagate near the surface on a large distance.

For the TM polarization and from Appendix A, we show that

$$P = \frac{i}{4} \sum_{n=0}^{\infty} \left(\frac{i}{k_0 \Delta}\right)^n \frac{\partial^n}{\partial z_2^n} H_0^{(1)}\left(k_0\sqrt{x_2^2 + z_2^2}\right). \quad (11)$$

For a highly-conducting surface, unlike the TE polarization, since $|\Delta| \to 0$ the sum converges very slowly, which makes the numerical evaluation of the sum very difficult. Thus, the above equation is not adequate to derive analytically P.

That is why for a two-dimensional (2-D) surface, Collin [1] addressed an asymptotic evaluation of integral (7) via the steepest descent method. In the recent paper of Koh *et al.* [5], for a 2-D surface, a closed-form expression of the Sommerfeld integral is also reported, in which special functions are involved in the sum. But, for $|\Delta|$ close to zero, the sum converges very slowly, and then the Collin solution is more appropriate for our application.

In Appendix B, this approach is summarized and applied to a 1-D surface. The resulting integral evaluation has then the same form as the one obtained for a 2-D surface

$$\frac{P^\infty}{g^\infty(r_2)} = -\alpha_2 \left[v\sqrt{\pi}\,\mathrm{erfc}(v)e^{v^2} \right] + \alpha_1 + \alpha_2 \qquad (12)$$

but the argument v and the terms $\{\alpha_1, \alpha_2\}$ are different and defined as

$$\begin{cases} v = e^{-i\pi/4} \sqrt{\frac{2k_0|x_2|}{\sin\theta}} \sin\left[\frac{\arccos(-\Delta)-\theta}{2}\right] \\ \alpha_1 = \frac{\Delta}{\Delta+\cos\theta} \\ \alpha_2 = \frac{-\Delta}{2\sqrt{1-\Delta^2}\cos\left(\frac{\theta}{2}+\frac{\arccos\Delta}{2}\right)} \end{cases} \qquad (13)$$

with the following condition

$$r_2 \geq \frac{2t_0^2}{4k_0 \left|\sin^2\left(\frac{\arccos(-\Delta)-\frac{\pi}{2}}{2}\right)\right|} \approx \frac{2t_0^2}{k_0|\Delta|^2} \qquad (14)$$

for $|\Delta| \to 0$. The value $t_0 > 1$ is of the order of 3 and will be optimized from the benchmark method presented in the next section.

For $|\Delta| \to 0$ and $\chi = \pi/2 - \theta \to 0$, (13) becomes

$$\begin{cases} v \approx e^{-i\pi/4} \sqrt{\frac{k_0|x_2|}{2}}(\Delta+\chi) \\ \alpha_2 \approx -\frac{\Delta}{\Delta+\chi} \\ \alpha_1 + \alpha_2 \approx 0 \end{cases} \qquad (15)$$

Moreover, if $\chi \ll |\Delta|$, then $\alpha_2 \approx -1$.

IV. RIGOROUS METHOD

This section presents a rigorous fast method based on the integral equations, which allows us to treat a very large problem. Indeed, to exhibit the ground wave, which propagates near the surface over a very large distance from the source point, the surface must be very large, typically, a few hundreds of kilometers. For a frequency of the order of 30 MHz ($\lambda_0 = 10$ m) and with a sampling step of $\lambda_0/10 = 1$ m, the number of unknowns on the surface must then be greater than $N_i = 100\,000$.

The field $\psi(\mathbf{r})$ and its normal derivative $\partial\psi(\mathbf{r})/\partial n_s$ on the surface are expressed from the integral equations [12] as

$$\begin{cases} \psi_i(\mathbf{r}') = -\int_S \frac{\partial g_0(\mathbf{r},\mathbf{r}')}{\partial n_s}\psi(\mathbf{r})dS + \int_S \frac{\partial\psi(\mathbf{r})}{\partial n_s}g_0(\mathbf{r},\mathbf{r}')dS \\ 0 = -\int_S \frac{\partial g_1(\mathbf{r},\mathbf{r}')}{\partial n_s}\psi(\mathbf{r})dS + \rho\int_S \frac{\partial\psi(\mathbf{r})}{\partial n_s}g_1(\mathbf{r},\mathbf{r}')dS \end{cases} \qquad (16)$$

where $\rho = 1$ for the TE polarization, and $\rho = n^2$ for the TM polarization. The scalar Green function of the lower medium is $g_1 = g(\sqrt{n}\,\|\mathbf{r}-\mathbf{r}'\|)$, whereas the one of the upper medium is $g_0 = g(\|\mathbf{r}-\mathbf{r}'\|)$.

Since the surface is assumed to be highly conducting ($|n| \gg 1$), the IBC (impedance boundary condition, also named Leon-

tovitch boundary condition) approximation can be applied. This leads to

$$\begin{cases} \psi(\mathbf{r}) = \frac{i}{k_0 n}\frac{\partial\psi(\mathbf{r})}{\partial n_s} & \text{(TE)} \\ \frac{\partial\psi(\mathbf{r})}{\partial n_s} = \frac{k_0}{in}\psi(\mathbf{r}) & \text{(TM)} \end{cases} \qquad (17)$$

Thus, substituting (17) into (16), for the TE polarization, only the field normal derivative is computed from the method of moments (MoM), and the field ψ is then computed from (17). For the TM polarization, the field ψ is computed from the MoM, and the field normal derivative is then computed from (17).

To solve numerically (16), the MoM [11] is applied. Then, using the MoM with point matching and pulse basis functions, a linear system $\bar{\mathbf{Z}}\mathbf{X} = \mathbf{b} \Rightarrow \mathbf{X} = \bar{\mathbf{Z}}^{-1}\mathbf{b}$ is obtained, in which $\bar{\mathbf{Z}}$ is the impedance matrix, $\mathbf{X}$ the vector containing the unknowns $\{\psi(\mathbf{r}_p), \partial\psi(\mathbf{r}_p)/\partial n_s\}$ sampled on the surface ($p \in [1, N_i]$, $\mathbf{r}_p \in S$) and $\mathbf{b}$ the vector containing the sampled incident field $\psi_i(\mathbf{r}_q)$ ($q \in [1, N_i]$, $\mathbf{r}_q \in S$). The elements of the impedance matrix can be found in [12]. Since the number of unknowns N_i is huge, a classical LU inversion to invert $\bar{\mathbf{Z}}$ can not be applied.

In the last two decades, rapid rigorous numerical methods, devoted to the scattering from rough surfaces, have been developed to solve this issue. For instance, one can cite the banded-matrix-iterative-approach/canonical grid (BMIA-CAG) of Tsang *et al.* [13], [14] of complexity $\mathcal{O}(N_i \log N_i)$, the Forward-Backward (FB) method of Holliday *et al.* [15] of complexity $\mathcal{O}(N_i^2)$, and the accelerated version, forward-backward spectral acceleration (FB-SA), of Chou *et al.* [16], [17] of complexity $\mathcal{O}(N_i)$. The principle of these methods is not to invert the impedance matrix but to replace $\bar{\mathbf{Z}}^{-1}\mathbf{b}$ by a succession of matrix-vector products. For more details, see [15], [16], [18], [19] for the FB-SA and see [13], [14], [20] for the BMIA-CAG. It can be noted that the later is very efficient for slightly rough surfaces, i. e. $\sigma_z/\lambda_0 \ll 1$, and *a fortiori* for a smooth surface. Moreover, the BMIA-CAG required the knowledge of two integers (i) The width of the strong interaction band matrix, $N_{s,\mathrm{BMIA}}$, which is much smaller than N_i (ii) The term number, P_{BMIA}, retained in the series expansion of the impedance matrix elements of the weak interactions.

For the TM polarization, Fig. 2 shows the ratio $|\psi^{\mathrm{BMIA-CAG}}/\psi^{\mathrm{LU}}|$ in dB scale ($20\log_{10}|\psi^{\mathrm{BMIA-CAG}}/\psi^{\mathrm{LU}}|$) versus the abscissa x. $\psi^{\mathrm{BMIA-CAG}}$ is the field on the surface computed from the BMIA-CAG, whereas ψ^{LU}, is the field computed from a direct LU inversion. The frequency $f = 30$ MHz $\Rightarrow \epsilon_r = 80 + 2400i \Rightarrow n = 35.2 + 34.1j$, the height of the emitter is $z_0 = 10$ m and its abscissa $x_0 = 0$ m. The number of unknowns is $N_i = 4000$ ($\Delta x = 1$ m and the surface length $L = 4$ km). In the legend, the labels give the order of the BMIA-CAG method (P_{BMIA}).

Fig. 3 plots the same variations as in Fig. 2 but for the TE polarization. For both polarizations, the number $N_{s,\mathrm{BMIA}} = 1$. As one can see, the BMIA-CAG method converges very rapidly for both polarizations and after only 1 iteration. In addition, the difference modulus does not exceed 4×10^{-5} dB for the TM polarization and 0.06 dB for the TE polarization. To obtain the high accuracy of interest here, the FB-SA requires a larger number of spectral integration points [17] that reduces the efficiency of the algorithm compared to BMIA-CAG for this problem.
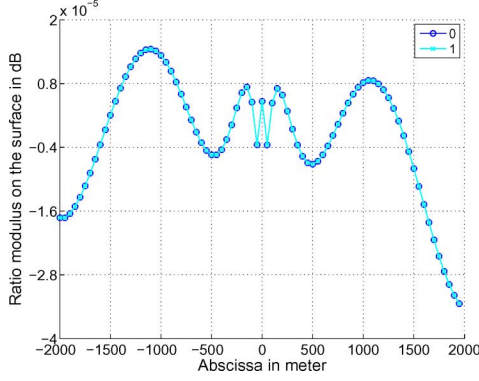
Fig. 2. Ratio $|\psi^{\mathrm{BMIA-CAG}}/\psi^{\mathrm{LU}}|$ in dB scale versus the abscissa. $f = 30$ MHz $\Rightarrow \epsilon_r = 80 + 2400i$, $z_0 = 10$ m, $x_0 = 0$ m, and $N_i = 4000$.
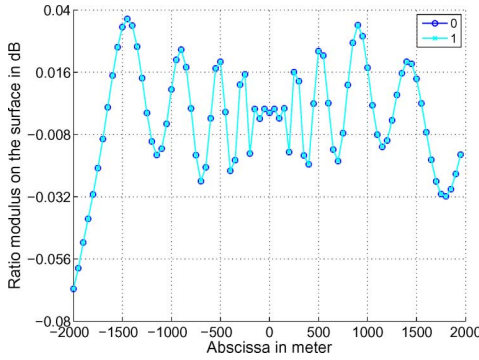

Fig. 3. Same as in Fig. 2 but for the TE polarization.

V. NUMERICAL RESULTS FOR A SMOOTH SEA SURFACE

In this section, numerical results are presented for a smooth sea surface in the HF-VHF band ($f \in [20; 100]$ MHz). In addition, the emitter is located at $(x_0, z_0) = (0, 10)$ m and the number of unknowns on the surface is $N_i = 262\,144$.

The scattered field is derived from the field and its normal derivative on the surface, computed from the BMIA-CAG, by applying the Huygens principle defined as

$$\psi_s(\mathbf{r}) = \int_{S'} \left[\frac{\partial g_0(\mathbf{r}, \mathbf{r}')}{\partial n_s} \psi(\mathbf{r}') - \frac{\partial \psi(\mathbf{r}')}{\partial n_s} g_0(\mathbf{r}, \mathbf{r}') \right] dS'. \quad (18)$$

From (6), the total scattered field can be written as

$$g_t(\mathbf{r}, \mathbf{r}_0) = \begin{cases} g(r_1) - g(r_2) + 2P & \text{(TE)} \\ g(r_1) - g(r_2) + 2F & \text{(TM)} \end{cases} \quad (19)$$

where $F = 1 - P$. Thus, for grazing angle ($\theta \to \pi/2$ or $x - x_0 \gg z + z_0$), $r_2 \approx r_1$ and $g_t \approx 2P$ for the TE polarization, whereas $g_t \approx 2F$ for the TM polarization.

From (18) and (19), the normalized functions P_N and F_N are computed from ($\psi_s = \psi_t - \psi_i = \psi_t - g(r_1)$)

$$\begin{cases} P_N = \frac{P}{g(r_2)} = \frac{\psi_s + g(r_2)}{2g(r_2)} & \text{(TE)} \\ F_N = \frac{F}{g(r_2)} = \frac{\psi_s + g(r_2)}{2g(r_2)} & \text{(TM)} \end{cases} \quad (20)$$
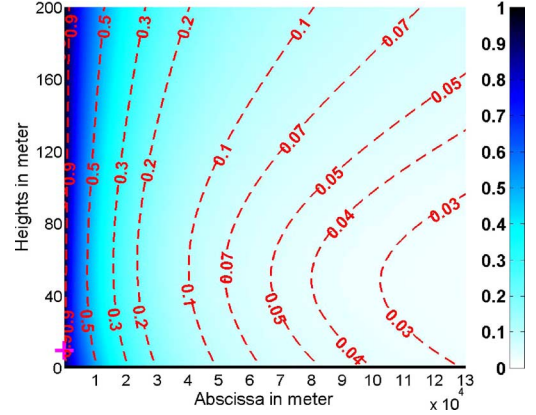

Fig. 4. Ratio $|F/g(r_2)|$ versus x and z for the TM polarization. $f = 30$ MHz $\Rightarrow \epsilon_r = 80 + 2400j$ MHz. The cross indicates the location of the emitter.

Fig. 4 plots the ratio $|F_N = F/g(r_2)|$ versus $x_2 = x - x_0$ and z for the TM polarization. $f = 30$ MHz $\Rightarrow \epsilon_r = 80 + 2400i$ and $L = 262.144$ km. The cross indicates the location of the emitter. Since the total scattered field is symmetrical with respect to x, only the part for $x \geq 0$ is shown.

As we can see, as the distance x increases, $|F_N|$ decreases very slowly and contributes near the surface. This behavior is characteristic of the ground wave and it is in qualitative agreement with (12). By contrast, numerical results not depicted here, clearly showed that for the TE polarization, the function $|P_N|$ vanishes. This means, that the total field vanishes since $g_t \approx 2P$. In other words, the surface finite conductivity does not affect the scattered field comparatively to a perfectly-conducting surface. This is in agreement with (10).

For the TM polarization, Fig. 5(a)-(b) show the real and the imaginary parts of F_N versus $u_2^{\mathrm{Re}} = x_2 \mathrm{Re}(-k_{zp}) = x_2 k_0 \mathrm{Re}(\Delta)$ ($x_2 = x - x_0 > 0$) for an observation height of $z = 10$ m. One obtains

$$f = \{30, 50, 70\} \text{ MHz} \Rightarrow \epsilon_r$$
$$= \{80 + 2400i, 80 + 1440i, 80 + 1029i\}.$$

The maximum value of $x = N_i \Delta x/2 = N_i \lambda_0/20 \approx \{131, 78, 56\}$ km.

It can be seen that the real part presents an oscillating behavior, for which the location of the minimum, $u_{2,\min}^{\mathrm{Re}}$, is independent of the frequency. This shows that the term $u_{2,\min}^{\mathrm{Re}} = x_{2,\min}^{\mathrm{Re}} k_0 \mathrm{Re}(\Delta) = \mathrm{cste}1$ is not sensitive to the frequency. Thus, as the frequency increases, the term $k_0 \mathrm{Re}(\Delta)$ increases, and thus the value of $x_{2,\min}^{\mathrm{Re}} = \mathrm{cste}1/(k_0 \mathrm{Re}(\Delta))$ decreases, which means that the real part of F_N decreases more fastly with the distance x_2. This behavior also holds for the maximum location of $\mathrm{Im}(F_N)$, i. e. $x_{2,\max}^{\mathrm{Im}} = \mathrm{cste}2/(k_0 \mathrm{Re}(\Delta))$. Using the same way, we can show that the amplitudes of the extrema are related to $\mathrm{Im}(k_{zp}) = k_0 \mathrm{Im}(\Delta)$. This means that the function $F_N(k_0, x_2, \Delta)$ can be expressed as $f(u, v) + jg(u, v)$, where $\{u = k_0 x_2 \mathrm{Re}(\Delta), v = k_0 x_2 \mathrm{Im}(\Delta)\}$ and the functions f and g are real. This new dependence allows us to reduce the number of freedom degrees. In addition, this result shows clearly that when the frequency increases, the contribution of the ground
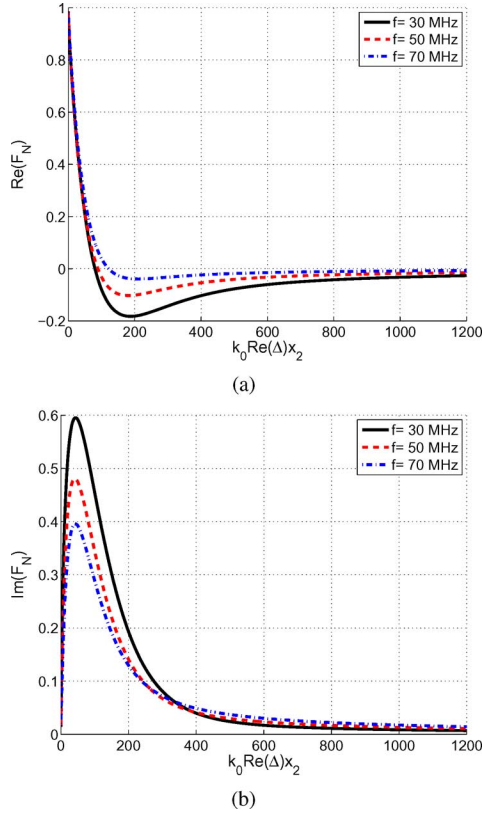
Fig. 5. (a) $\mathrm{Re}(F_N)$ versus $u_2^{\mathrm{Re}} = x_2 \mathrm{Re}(-k_{zp}) = x_2 k_0 \mathrm{Re}(\Delta)$ for the TM polarization and for an observation height of $z = 10$ m and $f = \{30, 50, 70\}$ MHz. (b) Same as in (a) but for the imaginary part, $\mathrm{Im}(F_N)$.
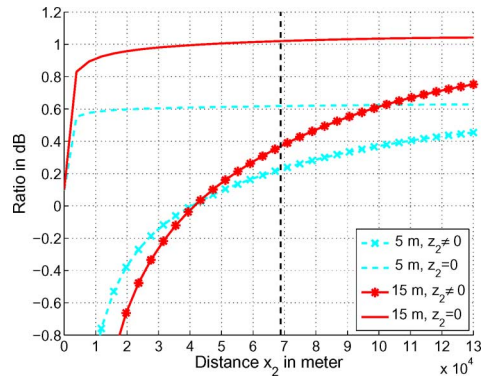

Fig. 6. $|20 \log_{10} |F_N^{\mathrm{BMIA\text{-}CAG}}/F_N^{\mathrm{Collin}}\||$ versus $x_2 = x - x_0$ for the TM polarization, for $f = 20$ MHz and for different observation heights.

wave decreases with the distance, which is in agreement with the experimental observations.

Fig. 6 plots $|20 \log_{10} |F_N^{\mathrm{Collin}}/F_N^{\mathrm{BMIA\text{-}CAG}}\||$ versus $x_2 = x - x_0$ for the TM polarization, for $f = 20$ MHz and for different observation heights ($z/\lambda_0 = \{0.33, 1.00\}$). F_N^{Collin} is computed from (12), whereas $F_N^{\mathrm{BMIA\text{-}CAG}}$ is computed from the BMIA-CAG. The vertical line gives the value of $x_2 = r_2 \sin \theta = 68.8$ km, for which the Collin formulation is valid. It was computed from (14) with $t_0 = 2$. In addition, Fig. 6 plots the curves for zeros receiver and emitter heights ($z_2 = z_0 + z = 0 \Rightarrow \theta = \pi/2$ in (12)).
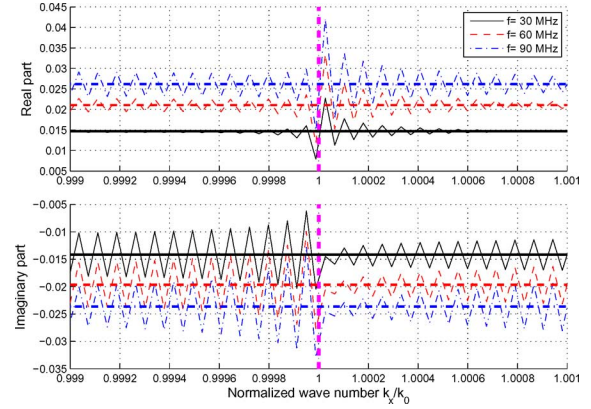

Fig. 7. Real and imaginary parts of $-v_{zp}(k_x)\sqrt{1-u^2} = \hat{\Delta}(k_x)$ versus $u = k_x/k_0$ and for $f = \{30, 60, 90\}$ MHz.

As expected for small distance x_2, the Collin approach can not be applied, and as x_2 increases, the results match better the BMIA-CAG ones. Moreover, the Collin formulation is better when the effect of the heights is included.

For very large distance, $\chi = \pi/2 - \theta \to 0$, and for $|\Delta| \to 0$, in (12), $\{v, \alpha_1, \alpha_2\}$ are given by (15), and v becomes large. In addition, the function $v\sqrt{\pi}\mathrm{erfc}(v)e^{v^2}$ behaves $1/(2v^2)$, and thus

$$P_N \approx \frac{\Delta i}{2(\Delta + \chi)^3 k_0 r_2} \approx \frac{i}{2\Delta^2 k_0 r_2}. \tag{21}$$

Equation (21) shows that, as the frequency increases, the normalized impedance modulus increases, and thus the function $|F_N|$ decreases. Fig. 6 also shows that when the observation height increases, the differences between the BMIA-CAG and the Collin results increase. This difference can not be attributed to the accuracy of the BMIA-CAG method because the field computed on the sea surface is independent of the observation height, and the scattered field is derived rigorously from the Huygens principle.

From (2) and for the TM polarization, the reflection coefficient is expressed in the Fourier domain as

$$\hat{\mathcal{R}}(k_x) = \frac{\hat{g}_s(k_x)}{\hat{g}_i(k_x)} = \frac{1 + v_{zp}(k_x)}{1 - v_{zp}(k_x)} \Leftrightarrow v_{zp}(k_x) = \frac{\hat{\mathcal{R}}(k_x) - 1}{\hat{\mathcal{R}}(k_x) + 1}. \tag{22}$$

In addition, $v_{zp} = k_{zp}/k_z = -\hat{\Delta}(k_x)/\sqrt{1-u^2}$, in which $u = k_x/k_0$ and $\hat{\Delta}(k_x)$ is expressed from (5). From the benchmark method, $\hat{\mathcal{R}} = (\hat{\psi} - \hat{\psi}_i)/\hat{\psi}_i$, where $\{\hat{\psi}, \hat{\psi}_i\}$ are the Fourier transforms of the total and incident fields on the surface, respectively, computed from the BMIA-CAG method.

Fig. 7 plots the real and imaginary parts of $-v_{zp}(k_x)\sqrt{1-u^2} = \hat{\Delta}(k_x)$ ($\approx \Delta$ for u close to 1) versus $u = k_x/k_0$ and for $f = \{30, 60, 90\}$ MHz. The horizontal bold lines correspond to the values of $\hat{\Delta}(k_x)$. As expected, for u close to 1, the quantity $-v_{zp}(k_x)\sqrt{1-u^2}$ is constant and equals Δ. With the BMIA-CAG method, this value is well predicted in terms of average value. Thus, from the total field on the surface, it is possible to calculate the surface normalized impedance. This way is very interesting and will be used to compute the surface normalized impedance from a rough surface.
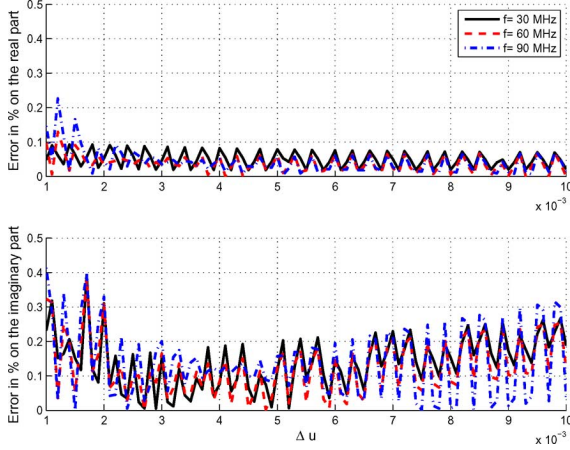
Fig. 8. Relative error in percent of $100 \times (\Delta - \Delta_{\mathrm{BMIA}})/\Delta$. At the top, the real part. At the bottom, the imaginary part.

TABLE I
VALUES OF P_{BMIA} AND $N_{s,\mathrm{BMIA}}$ FOR THE
TM POLARIZATION AND FOR $f = 30$ MHz

u_{10} in m/s	0	3	5	7	10
P_{BMIA}	1	2	2	3	3
$N_{s,\mathrm{BMIA}}$	2	3	3	3	4

To optimize the calculation of Δ from the BMIA-CAG method, Fig. 8 plots the real and imaginary parts of the relative error in percent, $100 \times (\Delta - \Delta_{\mathrm{BMIA}})/\Delta$, versus δu. Δ_{BMIA} is the mean value of $-v_{zp}(k_x)\sqrt{1-u^2}$ computed over $u \in [1 - \delta u; 1 + \delta u]$ with the BMIA-CAG. In Fig. 7, $\delta u = 0.001$. It can be seen, for u close to 1 (δu close to 0), the error does not exceed 0.2% and 0.4% for the real and imaginary parts, respectively, and the value $\delta u = 0.004$ is a good choice.

VI. NUMERICAL RESULTS FOR A ROUGH SEA SURFACE

In this section, a rough sea surface is considered. The rough surface height is assumed to be a Gaussian stationary stochastic process with zero mean value, and the height spectrum obeys the Elfouhaily *et al.* hydrodynamic spectrum [21], in which the key parameter is the wind speed u_{10} at 10 meters above the sea surface. In an electromagnetic point of view, in HF-VHF band, since the ratio σ_z/λ_0 is much smaller than one, the surface is slightly rough. From the Elfouhaily spectrum, Bourlier *et al.* [22] showed that the height standard deviation is $\sigma_z \approx 6.29 \times 10^{-3} u_{10}^{2.02}$. For instance for $u_{10} = 5$ m/s (Beaufort scale 4–5), $\sigma_z = 0.16$ m, which implies that the ratio $\sigma_z/\lambda_0 \in [0.011; 0.053]$ for $f \in [20; 100]$ MHz. Thus, the BMIA-CAG method is very efficient because its order P_{BMIA} and its strong interaction band width $N_{s,\mathrm{BMIA}}$ are proportional to this ratio. Table I reports these values used for the next simulations, and they are obtained by using the same way as a smooth surface (see Section IV).

By using a spectral method, several independent surfaces (but with a same Gaussian process and a same height spectrum) are generated. For each surface numbered p, the field ψ_p and its normal derivative $\partial \psi_p/\partial n_s$ are computed, and then from (18)
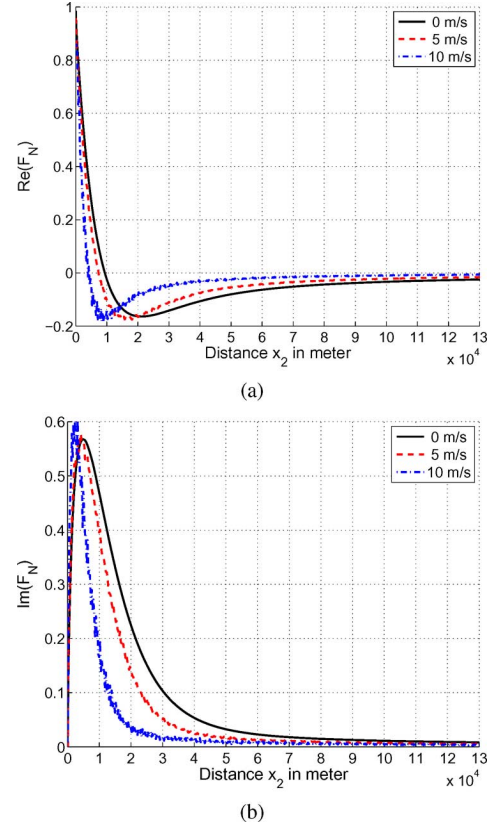

Fig. 9. (a) $\mathrm{Re}\,\langle F_N \rangle$ versus $x_2 = x - x_0$ for the TM polarization and for an observation height of $z = 15$ m. (b) Same as in (a) but for $\mathrm{Im}\,\langle F_N \rangle$. $f = 30$ MHz, $u_{10} = 0, 5, 10$ m/s, and $N_r = 10$.

and (20), the scattered field $\psi_{s,p}$ and the function $F_{N,p}$ are computed. The average of F_N, denoted as $\langle F_N \rangle$ is then obtained from

$$\langle F_N \rangle = \frac{1}{N_r} \sum_{p=1}^{p=N_r} F_{N,p} \qquad (23)$$

where N_r is the number of realizations.

Fig. 9(a)-(b) show $\mathrm{Re}\,\langle F_N \rangle$ and $\mathrm{Im}\,\langle F_N \rangle$, respectively, versus $x_2 = x - x_0$ for the TM polarization and for an observation height of $z = 15$ m. $f = 30$ MHz and $N_r = 10$.

As the wind speed increases, the distance over which the surface wave propagates decreases significantly. Thus, the surface roughness strongly affects the propagation. This behavior is in agreement with the results reported by Ishimaru *et al.* [8]. They showed from an asymptotic perturbative theory and for a *Gaussian* spectrum, that the coherent field decreases faster with respect to x_2 than the one of a smooth surface. Fig. 9(a)-(b) also show that the roughness has a minor impact on the extrema amplitude, which means that the pole imaginary part, related to the damping, is less affected by the surface roughness than the pole real part.

Fig. 10 represents the same variations as in Fig. 9(a) but for the modulus, $|\langle F_N \rangle|$ and versus $x_2\nu$. The ratio ν is defined as $\nu = x_{20}^{\mathrm{smooth}}/x_{20}^{\mathrm{rough}}$, in which x_{20} is the value of $|\langle F_N \rangle|$ for a given threshold s_0. The superscripts $\{\mathrm{smooth}, \mathrm{rough}\}$ refer to smooth and rough surfaces, respectively. Fig. 11 plots the ratio ν versus u_{10}^2 for a threshold $s_0 = 0.1$ and for three observation heights. One can see that the curves coincide. This confirms that
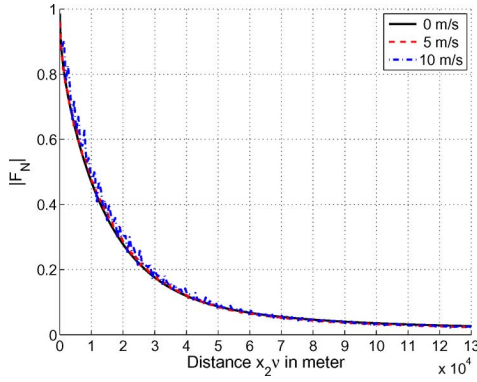
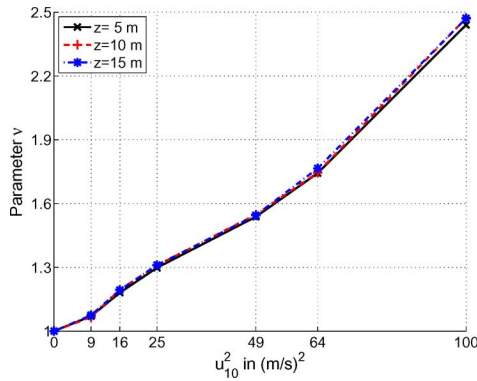Fig. 10. Same as in Fig. 9(a) but for the modulus, $|\langle F_N \rangle|$ and versus $x_2\nu$. $f = 30$ MHz.

Fig. 11. Ratio ν versus the wind speed u_{10} for a threshold $s_0 = 0.1$. $f = 30$ MHz.
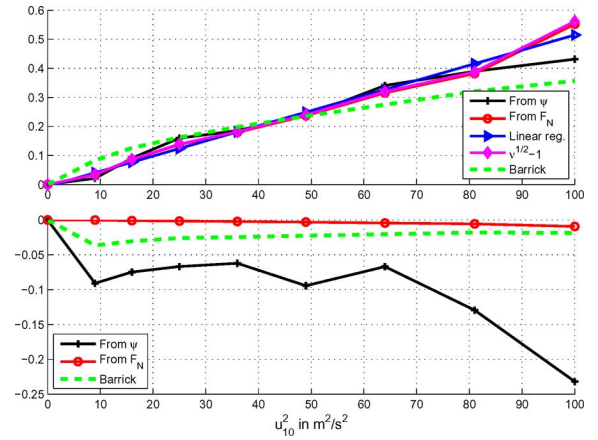

Fig. 12. $\Delta^{\text{rough}}/\Delta^{\text{smooth}} - 1 = a + ib$ versus u_{10}^2. At the top, the real part a. At the bottom, the imaginary part b. $f = 30$ MHz.
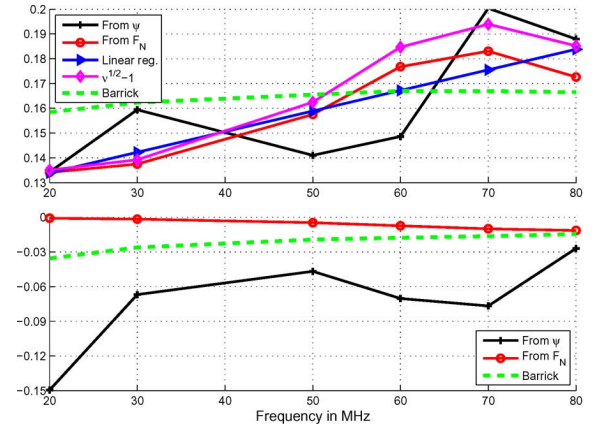

Fig. 13. $\Delta^{\text{rough}}/\Delta^{\text{smooth}} - 1 = a + ib$ versus the frequency f in MHz. At the top, the real part a. At the bottom, the imaginary part b. $u_{10} = 5$ m/s.

the roughness affects only the real part of the pole, and then $\text{Re}(k_{zp}^{\text{rough}}) \approx \text{Re}(k_{zp}^{\text{smooth}})\nu$ with $\nu \geq 1$.

Fig. 11 also shows that ν is slightly sensitive to the observation height, revealing that ν does not depend on the scattered field ψ_s, and it is rather an intrinsic property of the field on the surface ψ, as the surface pole. In addition, ν is strongly related to u_{10}^2 or to the standard deviation $\sigma_z \approx 6.29 \times 10^{-3} u_{10}^{2.02}$.

From an asymptotic perturbative theory, Ishimaru *et al.* [8] showed that the coherent attenuation function $\langle F_N \rangle$ keeps the same form as the one of a smooth surface, but with a new pole ([8, Eq. (46)]), as functions of the smooth surface pole and of the sea roughness spectrum. In other words, the pole of a rough surface can be expressed as $k_{zp}^{\text{rough}} \approx k_{zp}^{\text{smooth}}(1 + a + ib)$, in which $(a, b) \in \mathbb{R}^2$ and $a = b = 0$ for $u_{10} = 0$. This relation also holds for the surface normalized impedance, that is to say $\Delta^{\text{rough}} \approx \Delta^{\text{smooth}}(1 + a + ib)$.

Several ways can be used to calculate a and b. First, they are computed from the field ψ on the surface (see the end of Section V, label "From ψ" in the legend of Fig. 12). Second, they are computed from (12) and (15) (label "From F_N" in the legend of Fig. 12). Indeed, (12) shows that F_N depends only on v if approximations (15) are valid. In this case, for a same threshold s_0, chosen such as (15) is valid, one has $v^{\text{smooth}} = v^{\text{rough}}$ leading to

$$\Delta^{\text{rough}} \approx \sqrt{\frac{x_{20}^{\text{smooth}}}{x_{20}^{\text{rough}}}} \left(\Delta^{\text{smooth}} + \chi^{\text{smooth}} \right) - \chi^{\text{rough}}$$

$$\chi = \arctan\left(\frac{z_2}{x_2} \right). \tag{24}$$

For $\chi \ll |\Delta|$, $\Delta^{\text{rough}}/\Delta^{\text{smooth}} \approx \sqrt{x_{20}^{\text{smooth}}/x_{20}^{\text{rough}}} = \sqrt{\nu}$, which is a real number.

Fig. 12 plots the ratio $\Delta^{\text{rough}}/\Delta^{\text{smooth}} - 1 = a + ib$ versus u_{10}^2 with $f = 30$ MHz. At the top, it can be seen that both methods predict similar results and like ν, the real part a is proportional to u_{10}^2. A linear regression leads to $a \approx -0.006444 + 0.005211 u_{10}^2$ (the regression coefficient is 0.99375) with $u_{10} \in [0; 10]$ m/s (label "Linear reg." in Fig. 12). At the bottom, the prediction of the imaginary part b differs from the method, but remains small comparatively to the real part a. Thus, as previously said, the roughness has a minor impact on the imaginary part of the surface normalized impedance or on the surface pole.

Fig. 12 also shows comparisons with the Barrick theory [6] ((22) applied to 1-D surfaces, i.e., $q = 0$) based on a perturbative method. For the real part, as the wind increases, the difference increases. Indeed, as the surface roughness increases, the use of a perturbative approach is questionable. For example, for $u_{10} = 7$ m/s, $k_0\sigma_z = 0.20$. For small wind speeds, a slightly difference also appears. For the imaginary part, as the BMIA-CAG, the Barrick asymptotic theory predicts levels much smaller than the real part.

Fig. 13 plots the ratio $\Delta^{\text{rough}}/\Delta^{\text{smooth}} - 1 = a + ib$ versus the frequency f in MHz. At the top, the real part a. At the bottom, the imaginary part b. The wind speed is $u_{10} = 5$ m/s. The
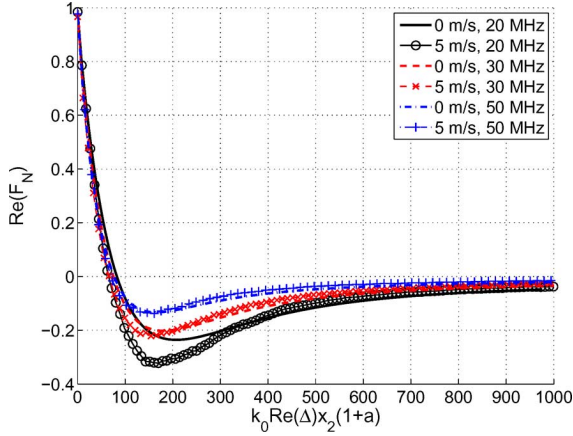
Fig. 14. $|\langle F_N \rangle|$ versus $k_0 x_2 \mathrm{Re}(\Delta)(1+a)$ for the TM polarization and for an observation height of $z = 15$ m. $u_{10} = \{0, 5\}$ m/s and $N_r = 10$.

definition of the labels is the same as in Fig. 12. As the frequency increases, the real part increases slightly. Comparatively to Fig. 12, this increasing is lower, which means that the ratio $\Delta^{\mathrm{rough}}/\Delta^{\mathrm{smooth}}$ is less sensitive to the frequency than the wind speed. As in Fig. 12, the imaginary part decreases very slowly with the frequency. In addition, these behaviors are in agreement with the Barrick results.

Figs. 12 and 13 reveal that the method with the label "From F_N" seems to be more accurate that the one with the label "From ψ". It can be explained by the fact that the field on the surface ψ presents oscillations, which makes the evaluation of the pole difficult. In addition, as the roughness increases (either the wind speed increases or/and the frequency increases), the coherent field decreases (the diffuse component increases), which makes the evaluation of the pole difficult because more surface realizations are necessary.

Fig. 14 represents $|\langle F_N \rangle|$ versus $k_0 x_2 \mathrm{Re}(\Delta)(1+a)$ $(x_2 = x - x_0)$ for the TM polarization and for an observation height of $z = 15$ m. $u_{10} = \{0(\mathrm{smooth}), 5\}$ m/s and $N_r = 10$. As expected, for a rough surface, the multiplication of the abscissa x_2 by $k_0 \mathrm{Re}(\Delta)(1+a)$ allows us to retrieve approximately the curves obtained for a smooth surface $(a = 0)$ and for a given frequency. The extremum level differs because the roughness also slightly modifies the imaginary part of the pole.

VII. CONCLUSION

For horizontally and vertically polarized line sources in HF-VHF band, analysis of the propagation over one-dimensional highly-conducting smooth and rough sea surfaces has been investigated from an efficient rigorous numerical method: the method of moments combined with the BMIA-CAG approach. For the TM polarization, the ground wave is then exhibited for smooth and rough sea surfaces, whereas for the TE polarization, such a wave can not be excited. The numerical results are compared with asymptotic theories based on the Sommerfeld integral.

For frequencies ranging from $f \in [10; 100]$ MHz, the main concluding remarks of this study are:

- The distance over which the ground waves propagates decreases when the frequency increases and the wind speed increases.
- Equations (12) and (13), which give an approached expression of the attenuation function $F_N = 1 - P_N$ and deduced from the Collin work, for which the antenna heights are assumed to be small in comparison to the wavelength, is valid for distance approximately greater than $4.5/(k_0|\Delta|^2)$, where k_0 is the incident wavenumber $(2\pi/\lambda_0)$ and Δ the surface normalized impedance expressed from (5).
- For a rough sea surface, the attenuation function keeps the same mathematical expression of the one of a smooth surface, in which the pole of a smooth surface, k_{zp}^{smooth}, must be replaced by k_{zp}^{rough} of the rough surface. In addition, the pole k_{zp}^{rough} can be approximated by $k_{zp}^{\mathrm{rough}} \approx k_{zp}^{\mathrm{smooth}}(1 + a + ib)$ with $(a, b) \in \mathbb{R}^2$.
- The real a is positive, slightly sensitive to the frequency and proportional to u_{10}^2.
- The real b is negative, much smaller than a in absolute value and its impact is minor on the attenuation function.

APPENDIX A
DERIVATION OF P

TM Polarization: For the TM polarization, the substitution of (4) into (7) leads to

$$P = \frac{ik_0\Delta}{4\pi} \int_{-\infty}^{+\infty} \frac{e^{ik_z z_2 + ik_x x_2} dk_x}{k_z (k_0\Delta + k_z)} \quad (A1)$$

where $x_2 = x - x_0$ and $z_2 = z + z_0$.

Using the Laplace transform

$$\frac{1}{k_0\Delta + k_z} = \int_0^\infty e^{-p(k_0\Delta + k_z)} dp \quad (A2)$$

one has

$$P = k_0\Delta \int_0^\infty e^{-pk_0\Delta} \left[\int_{-\infty}^{+\infty} \frac{i}{4\pi k_z} e^{ik_z(z_2 + jp) + ik_x x_2} dk_x \right] dp$$
$$= \frac{ik_0\Delta}{4} \int_0^\infty e^{-pk_0\Delta} H_0^{(1)} \left(k_0 \sqrt{x_2^2 + (z_2 + ip)^2} \right) dp$$
$$= \frac{i}{4} \int_0^\infty e^{-s} H_0^{(1)} \left(k_0 \sqrt{x_2^2 + \left(z_2 + \frac{is}{k_0\Delta} \right)^2} \right) ds, \quad (A3)$$

where $s = pk_0\Delta$. Unfortunately, it is very difficult to obtain a closed-form expression of the above integral.

Doing a succession of integrations by parts, we show that

$$P = \frac{i}{4} \sum_{n=0}^\infty \frac{\partial^n}{\partial s^n} H_0^{(1)} \left(k_0 \sqrt{x_2^2 + \left(z_2 + \frac{is}{k_0\Delta} \right)^2} \right) \Bigg|_{s=0}$$
$$= \frac{i}{4} \sum_{n=0}^\infty \left(\frac{i}{k_0\Delta} \right)^n \frac{\partial^n}{\partial z_2^n} H_0^{(1)} \left(k_0 \sqrt{x_2^2 + z_2^2} \right). \quad (A4)$$

For a highly-conducting surface, since $|\Delta| \to 0$ the sum converges very slowly, which makes the numerical evaluation of the integral very difficult.

TE Polarization: For the TE polarization, the substitution of (4) into (7) leads to

$$P = \frac{i\Delta}{4\pi} \int_{-\infty}^{+\infty} \frac{k_z}{k_0} \frac{e^{ik_z z_2 + ik_x x_2} dk_x}{k_z \left(1 + \Delta \frac{k_z}{k_0}\right)}. \tag{A5}$$

Using the variable transformations $\{x_2 = r_2 \sin\theta, z_2 = r_2 \cos\theta\}$ and $\{k_x = k_0 \sin\xi, k_z = k_0 \cos\xi\}$, one has

$$P = \frac{i\Delta}{4\pi} \int_{\Gamma} \frac{\cos\xi \, e^{ik_0 r_2 \cos(\theta-\xi)} d\xi}{1 + \Delta \cos\xi} \tag{A6}$$

where Γ is the integration contour of the scalar Green function in the complex plane defined as $\Gamma =]+i\infty; -\pi/2] \cup]-\pi/2; +\pi/2[\cup [+\pi/2; -i\infty[$. Series expansion over $\Delta \cos\xi$ around zero of the fraction leads to

$$P = \frac{i\Delta}{4\pi} \sum_{n=0}^{\infty} (-\Delta)^n \int_{\Gamma} e^{ik_0 r_2 \cos(\theta-\xi)} \cos^{n+1}(\xi) d\xi. \tag{A7}$$

In addition, since

$$g(r_2) = \frac{i}{4\pi} \int_{\Gamma} e^{ik_0 r_2 \cos(\theta-\xi)} d\xi \tag{A8}$$

and $r_2 \cos(\theta - \xi) = x_2 \sin\xi + z_2 \cos\xi$, one has

$$P = -\sum_{n=1}^{\infty} \left(\frac{i\Delta}{k_0}\right)^n \frac{\partial^n}{\partial z_2^n} g(r_2). \tag{A9}$$

For a highly-conducting surface, since $|\Delta| \to 0$ the sum converges very rapidly.

APPENDIX B
EVALUATION OF P FROM THE COLLIN APPROACH

In this appendix, the Collin approach [1] is summarized and applied to a 1-D surface.

Let us consider the following integral

$$\Omega = K \int_{\Gamma} \frac{G_n(\xi)}{G_d(\xi)} e^{ik_0 r_2 \cos(\theta-\xi)} d\xi \tag{B1}$$

where $G_d(\xi)$ is a function having a *simple single* zero defined for ξ_p, and Γ is the contour of the scalar Green function in the complex plane defined as $\Gamma =]+i\infty; -\pi/2] \cup]-\pi/2; +\pi/2[\cup [+\pi/2; -i\infty[$.

First, the integration contour of the integral is converted to the steepest-descent contour (SDC) leading to

$$\Omega \approx K e^{ik_0 r_2} \int_{\text{SDC}} G(\lambda) e^{-k_0^2 r_2^2 \lambda^2/2} d\lambda \tag{B2}$$

where

$$G(\lambda) = \frac{G_n(\lambda)}{G_d(\lambda)} \frac{d\xi}{d\lambda} \tag{B3}$$

and

$$\lambda(\xi) = 2e^{i\pi/4} \sin\left(\frac{\xi-\theta}{2}\right) \qquad \frac{d\xi}{d\lambda} = \frac{e^{-i\pi/4}}{\cos\left(\frac{\xi-\theta}{2}\right)}. \tag{B4}$$

Collin then showed that

$$\frac{\Omega}{g^{\infty}(r_2)} \approx -\alpha_2 \left[v\sqrt{\pi}\,\text{erfc}(v)e^{v^2}\right] + \alpha_1 + \alpha_2 \tag{B5}$$

where

$$\begin{cases} \alpha_1 = \frac{K_1 G(\xi=\theta)}{2} & \alpha_2 = \frac{K_1}{2\lambda(\xi_p)} \frac{G_n(\xi_p)}{\frac{dG_d}{d\xi}\big|_{\xi=\xi_p}} \\ K_1 = \frac{Ke^{ik_0 r_2}}{g^{\infty}(r_2)}\sqrt{\frac{2\pi}{k_0 r_2}} = 4K\pi e^{-i\pi/4} \\ v = e^{-i\pi/4}\sqrt{\frac{2k_0|x_2|}{\sin\theta}}\sin\left(\frac{\xi-\theta}{2}\right) \end{cases}. \tag{B6}$$

In our case, the following integral must be derived

$$P = \frac{i\Delta}{4\pi} \int_{-\infty}^{+\infty} \frac{e^{ik_z z_2 + ik_x x_2} dk_x}{k_z \left(\Delta + \frac{k_z}{k_0}\right)} = \frac{i\Delta}{4\pi} \int_{\Gamma} \frac{e^{ik_0 r_2 \cos(\theta-\xi)} d\xi}{\cos\xi + \Delta}. \tag{B7}$$

Thus, from (B1), we have $K = (i\Delta)/(4\pi)$, $G_n(\xi) = 1$, $G_d(\xi) = \cos\xi + \Delta$ and $\xi_p = \arccos(-\Delta)$, leading from (B6) to

$$\begin{cases} v = e^{-i\pi/4}\sqrt{\frac{2k_0|x_2|}{\sin\theta}}\sin\left[\frac{\arccos(-\Delta)-\theta}{2}\right] \\ \alpha_1 = \frac{\Delta}{\Delta+\cos\theta} \\ \alpha_2 = \frac{-\Delta}{2\sqrt{1-\Delta^2}\cos\left(\frac{\theta}{2}+\frac{\arccos\Delta}{2}\right)} \end{cases}. \tag{B8}$$

ACKNOWLEDGMENT

REFERENCES

[1] R. E. Collin, "Hertzian dipole radiating over a lossy earth or sea: Some early and late 20th-century controversies," *IEEE Antennas Propag. Mag.*, vol. 46, no. 2, pp. 64–79, 2004.

[2] J. R. Wait, "The ancient and modern history of EM ground-wave propagation," *IEEE Antennas Propag. Mag.*, vol. 40, no. 5, pp. 7–39, 1998.

[3] K. Sarabandi, M. D. Casciato, and I.-S. Koh, "Efficient calculation of the fields of a dipole radiating above an impedance surface," *IEEE Trans. Antennas Propag.*, vol. 50, no. 9, pp. 1222–1235, 2002.

[4] K. Sarabandi and I.-S. Koh, "Fast multipole representation of Green's function for an impedance half-space," *IEEE Trans. Antennas Propag.*, vol. 52, no. 1, pp. 296–301, 2004.

[5] I.-S. Koh and J. Yook, "Exact closed-form expression of a Sommerfeld integral for the impedance half-space Problem," *IEEE Trans. Antennas Propag.*, vol. 54, no. 9, pp. 2568–2576, 2006.

[6] D. E. Barrick, "Theory of HF and VHF propagation across the rough sea, 1, The effective surface impedance for a slightly rough highly conducting medium at grazing incidence," *Radio Sci.*, vol. 6, no. 5, pp. 517–526, 1971.

[7] D. E. Barrick, "Theory of HF and VHF propagation across the rough sea, 2, Application to HF and VHF propagation above the sea," *Radio Sci.*, vol. 6, no. 5, pp. 527–533, 1971.

[8] A. Ishimaru, J. D. Rockway, Y. Kuga, and S.-W. Lee, "Sommerfeld and Zenneck wave propagation for a finitely conducting one-dimensional rough surface," *IEEE Trans. Antennas Propag.*, vol. 48, no. 9, pp. 1475–1484, 2000.

[9] A. Ishimaru, J. D. Rockway, Y. Kuga, and S.-W. Lee, "Transverse electric and magnetic Green's function for coherent and incoherent propagation over a finitely conducting rough surface," *Radio Sci.*, vol. 37, no. 3, pp. 1–14, 2002.

[10] J. V. Toporkov and M. A. Sletten, "Numerical study of wide-band low-grazing HF clutter from ocean-like surfaces," in *IEEE Antennas and Propagation Society Int. Symp.*, 2005, vol. 1A, pp. 388–391.

[11] F. Harrington, *Field Computation by Moment Methods*. Piscataway, NJ: IEEE Press, 1993.

[12] L. Tsang, J. A. Kong, K.-H. Ding, and C. O. Ao, *Scattering of Electromagnetics Waves: Numerical Simulations*. New York: Wiley Interscience, 2001.

[13] L. Tsang, C. H. Chang, and H. Sangani, "A banded matrix iterative approach to monte carlo simulations of scattering of waves by large scale random rough surface problems: TM case," *Electron. Lett.*, vol. 29, pp. 1666–1667, 1993.

[14] L. Tsang, C. H. Chang, H. Sangani, A. Ishimaru, and P. Phu, "A banded matrix iterative approach to Monte Carlo simulations of large scale random rough surface scattering: TE case," *J. Electromagn. Waves Appl.*, vol. 29, pp. 1185–1200, 1993.

[15] D. Holliday, L. L. DeRaad Jr., and G. J. St-Cyr, "Forward-Backward: A new method for computing low-grazing angle scattering," *IEEE Trans. Antennas Propag.*, vol. 44, no. 1, pp. 1199–1206, 1995.

[16] H. T. Chou and J. T. Johnson, "A novel acceleration algorithm for the computation of scattering from rough surfaces with the Forward-Backward method," *Radio Sci.*, vol. 33, pp. 1277–1287, 1998.

[17] D. Torrungrueng, J. T. Johnson, and H. T. Chou, "Some issues related to the novel spectral acceleration method for the fast computation of radiation/scattering from one-dimensional extremely large scale quasi-planar structures," *Radio Sci.*, vol. 37, no. 2, pp. 1–20, 2002.

[18] N. Déchamps and C. Bourlier, "Electromagnetic scattering from a rough layer: Propagation-inside-layer expansion method combined to the forward-backward novel spectral acceleration," *IEEE Trans. Antennas Propag.*, vol. 55, no. 12, pp. 3576–3586, 2007.

[19] C. Bourlier, G. Kubické, and N. Déchamps, "A fast method to compute scattering by a buried object under a randomly rough surface: PILE combined with FB-SA," *J. Opt. Soc. Am. A*, vol. 25, no. 4, pp. 891–902, 2008.

[20] N. Déchamps and C. Bourlier, "Electromagnetic scattering from a rough layer: Propagation-inside-layer expansion method combined to an updated BMIA/CAG approach," *IEEE Trans. Antennas Propag.*, vol. 55, no. 10, pp. 2790–2802, 2007.

[21] T. Elfouhaily, B. Chapron, K. Katsaros, and D. Vandermark, "A unified directional spectrum for long and short wind-driven waves," *J. Geophys. Res.*, vol. 102, no. C7, pp. 781–796, 1997.

[22] C. Bourlier and G. Berginc, "Microwave analytical backscattering models from randomly rough anisotropic sea surface comparison with experimental data in C and Ku bands," *Progr. Electromagn. Res.*, vol. 37, pp. 31–78, 2002.

[23] K. A. Norton, "The calculation of ground-Wave field intensity over a finitely conducting spherical earth," *Proc. IRE*, pp. 623–639, 1941.

[24] I. S. Gradshteyn and L. M. Ryzbik, *Table of Integrals, Series and Products*, Sixth ed. New York: Academic Press, 2000.

Christophe Bourlier (M'99) was born in La Flèche, France, on July 6, 1971. He received the M.S. degree in electronics from the University of Rennes, France, in 1995 and the Ph.D. degree from the Polytech'Nantes (University of Nantes, France), in 1999.

While at the University of Rennes, he was with the Laboratory of Radiocommunication where he worked on antennas coupling in the VHF-HF band. Currently, he is with IREENA Laboratory (Institut de Recherche en Electrotechnique et Electronique de Nantes Atlantique, France) in the SEC team at Polytech'Nantes (University of Nantes, France). He works as an Assistant Researcher of National Center for Scientific Research on electromagnetic wave scattering from rough surfaces and objects for remote sensing applications. He is author of more than 120 journal articles and conference papers.

Gildas Kubické was born in Longjumeau, France, in September 1982. He received the Engineering degree and M.S. degree in electronics and electrical engineering both in 2005 and the Ph.D. degree in 2008 from the University of Nantes, France.

He is currently a Research Engineer in the SEC Team of IREENA Laboratory (Institut de Recherche en Electrotechnique et Electronique de Nantes Atlantique, France) at Polytech'Nantes (University of Nantes, France). His research interest includes electromagnetic scattering and radar cross section modeling.

Yohann Brelet was born in Nantes, France, in 1979. He received the M.S. degree in electronics and electrical engineering and the Ph.D. degree from the Polytech'Nantes (University of Nantes, France), in 2005 and 2008, respectively.

He is currently in a Postdoctoral position at the Laboratory of Physique Subatomique et des Technologies associées (Subatech) at Ecole des Mines de Nantes, France. His research interests are focused on non-destructive evaluation, laser ultrasonics and electromagnetic wave scattering from rough surfaces.